JOURNAL OF GUIDANCE, CONTROL, AND DYNAMICS
Vol. 33, No. 6, November–December 2010

Nonlinear Estimation of Hypersonic State Trajectories in Bayesian Framework with Polynomial Chaos

Parikshit Dutta* and Raktim Bhattacharya†
Texas A&M University, College Station, Texas 77843-3141

DOI: 10.2514/1.49743

This paper presents a nonlinear estimation algorithm to estimate state trajectories of a hypersonic vehicle with initial condition uncertainty. Polynomial chaos theory is used to predict the evolution of state uncertainty of the nonlinear system, and a Bayesian estimation algorithm is used to estimate the posterior probability density function of the nonlinear random process. The nonlinear estimation algorithm is then applied to the hypersonic reentry of a spacecraft in Martian atmosphere. Its performance is compared with estimators based on an extended Kalman filtering and unscented Kalman filtering framework. It is observed that for the particular application, the proposed estimator outperforms extended Kalman filtering and unscented Kalman filtering, highlighting its need in the current scenario.

I. Introduction

HYPERSONIC flight leading to entry descent landing of a large spacecraft on the surface of Mars has been identified as a research area by NASA. Expected mass of the next Mars Science Laboratory mission is approximately 2800 kg at entry, which is required to land within a few kilometers of the robotic test sites. One of the major concerns of high mass entry is the mismatch between entry conditions and deceleration capabilities provided by supersonic parachute technologies. In such applications, there are uncertainties present in initial conditions and other system parameters. Estimation of parameters for these systems is a hard problem because of the nonlinearities in the system and the lack of frequent measurements. The evolution of uncertainty, which can be non-Gaussian, needs to be predicted over longer intervals of time. Hence, the classical linear Gaussian theory does not provide solutions with acceptable accuracy. The main challenges of nonlinear estimation are in the prediction of uncertainty for nonlinear dynamical systems and its correction based on measurements.

State estimation is usually performed in the Bayesian framework where uncertainty in the parameter is represented in terms probability density functions (PDFs). Bayesian parameter estimation for linear Gaussian systems is optimal with Kalman filters [1,2]. For nonlinear systems exhibiting Gaussian behavior, the system is linearized locally, about the current mean, and the covariance is propagated using the approximated linear dynamics. This method is used in extended Kalman filters (EKFs) [2,3]. It is well known that this approach performs poorly when nonlinearities are high resulting in an unstable estimator [4–7]. However, the error in mean and covariance can be reduced if the uncertainty is propagated using the nonlinear dynamics for a set of sample points, called sigma points. The probability density function of the states is parameterized by the sigma points, completely capturing the true mean and covariance. When propagated through the true nonlinear system, this approximated density function captures the posterior mean and covariance accurately to the third order (Taylor series expansion) for any nonlinearity with Gaussian behavior. This technique has resulted in the unscented Kalman filter (UKF) [8]. Recently, simulation-based sequential estimation algorithms based on Monte Carlo simulations have been proposed to tackle nonlinear systems with non-Gaussian uncertainties [9–12]. Among them, the most widely used is the particle filter [13,14]. In this method, ensemble members (also called *particles*) are propagated using the nonlinear system. The particles, properly weighted based on measurements, are used to obtain the state estimate. Since the particle filter is based on Monte Carlo simulations, the ensemble size scale exponentially with state dimension when problem size is large [15].

In this paper, an estimation algorithm based in the framework of Bayesian inference has been proposed. Polynomial chaos theory is used to propagate uncertainty in a nonlinear dynamical system, and the state estimate is obtained by minimizing the covariance of the posterior probability distribution. As described later, the computational complexity of polynomial chaos grows factorially with the dimension of unknown parameters. However, it has been shown that PC is computationally more efficient than Monte Carlo simulations [16]. Based on this fact, it is expected that the estimation algorithm presented here will be computationally more efficient than particle filters. However, such an analysis has not been performed in this paper and is a subject of our future work.

Polynomial chaos was first introduced by Wiener [17] where Hermite polynomials were used to model stochastic processes with Gaussian random variables. According to Cameron and Martin [18], such an expansion converges in the $\mathcal{L}_2$ sense for any arbitrary stochastic process with finite second moment. This applies to most physical systems. Xiu and Karniadakis [16] generalized the result of Cameron and Martin [18] to various continuous and discrete distributions using orthogonal polynomials from the so-called Askey scheme [19] and demonstrated $\mathcal{L}_2$ convergence in the corresponding Hilbert functional space. This is popularly known as the generalized polynomial chaos (gPC) framework. The gPC approach is *limited to parametric uncertainty* and cannot be used to study the effect of stochastic forcing directly. However, stochastic forcing processes that have nonzero correlation window, can be approximated to arbitrary accuracy using the Karhunen–Loeve expansions. This approximates the random process using known functions of time with coefficients that are random variables, thus transforming it to a problem with parametric uncertainty. The problem then becomes amenable for analysis in the gPC framework. The gPC framework has been applied to various applications, including stochastic fluid dynamics [20,21], stochastic finite elements [22], and solid mechanics [23,24]. Application of gPC to problems related to control and estimation of dynamical systems has been surprisingly limited [25–30].

In the context of nonlinear estimation, polynomial chaos has been applied by Sandu et al. [31,32], where uncertainty prediction was computed using gPC theory for nonlinear dynamical systems, and

Received 5 March 2010; revision received 7 May 2010; accepted for publication 7 May 2010.

*Graduate Student, Aerospace Engineering Department; p0d5585@aero.tamu.edu.

†Assistant Professor, Aerospace Engineering Department; raktim@aero.tamu.edu.

estimation was performed using linear output equations and classical Kalman filtering theory. This paper combines gPC theory with Bayesian estimation and develops a new estimation method for non-Gaussian nonlinear processes. The proposed method was applied to estimate states of hypersonic reentry dynamics in Martian atmosphere with Gaussian initial condition uncertainty. For such a system, uncertainty does not remain Gaussian throughout the propagation time; hence, EKF- and UKF-based methods are expected to perform poorly. As mentioned before, the limitation of gPC theory is that it can only incorporate parametric uncertainty in the system, which is the premise of the estimation algorithm presented here.

The paper is organized as follows. First, the polynomial chaos theory is introduced and is used demonstrate how differential equations with initial state uncertainty can be solved in gPC framework. This is followed by the details of estimation algorithm that combine gPC theory and Bayesian estimation. The developed estimator is then applied to hypersonic reentry flight dynamics and its performance is compared with estimators built in the EKF and UKF frameworks.

II. Wiener–Askey Polynomial Chaos

A. Generalized Polynomial Chaos Theory

Let $(\Omega, \mathcal{F}, \mathcal{M})$ be a probability space, where Ω is the sample space, $\mathcal{F}$ is the σ algebra of the subsets of Ω, and $\mathcal{M}$ is the probability measure. Let

$$\Delta(\omega) = (\Delta_1(\omega), \ldots, \Delta_d(\omega)) \colon (\Omega, \mathcal{F}) \to (\mathbb{R}^d, \mathcal{B}^d)$$

be an $\mathbb{R}^d$-valued continuous random variable, where $d \in \mathbb{N}$, and $\mathcal{B}^d$ is the σ algebra of Borel subsets of $\mathbb{R}^d$. A general second-order process $X(\omega) \in \mathcal{L}_2(\Omega, \mathcal{F}, \mathcal{M})$ can be expressed in polynomial chaos framework as

$$X(\omega) = \sum_{i=0}^{\infty} x_i \phi_i(\Delta(\omega)) \tag{1}$$

where ω is the random event and $\phi_i(\Delta(\omega))$ denotes the gPC basis function of degree i, in terms of the random variables $\Delta(\omega)$. Henceforth, Δ will be used to represent $\Delta(\omega)$. Given the random variable Δ with PDF, $p(\Delta)$, let $v = [1, \Delta, \Delta^2, \ldots, \infty]^T$. The family of orthogonal basis functions $\{\phi_i(\Delta)\}$ are given by

$$\phi_0(\Delta) = v_0 \tag{2a}$$

$$\phi_i(\Delta) = v_i - \sum_{k=0}^{i-1} \frac{\langle v_i, \phi_k(\Delta)\rangle}{\langle \phi_k(\Delta), \phi_k(\Delta)\rangle} \phi_k(\Delta) \qquad i = 1, \ldots, \infty \tag{2b}$$

where

$$\langle \phi_i, \phi_j \rangle = \int_{\mathcal{D}_\Delta} \phi_i \phi_j p(\Delta)\, \mathrm{d}\Delta$$

where $\langle \cdot, \cdot \rangle$ denotes the inner product with respect to the weight function $p(\Delta)$, and $\mathcal{D}_\Delta$ is the domain of the random variable Δ. Note that the weight function for the inner product here is same as the PDF of Δ.

The procedure in Eq. (2) is the classical *Gram–Schmidt orthogonalization* [33]. The orthogonal polynomials thus obtained are the members of the Askey scheme of polynomials [19], which form a complete basis in the Hilbert space determined by their corresponding support. Table 1 summarizes the correspondence between the orthogonal polynomials for a given PDF of Δ [16].

B. Approximation of the Solution of Ordinary Differential Equations with Uncertainty

A dynamical system of the form $\dot{x} = f(x, \Delta)$, where $x \in \mathbb{R}^n$ and random variable $\Delta \in \mathbb{R}^d$, representing uncertainty in initial states and parameters, can be solved in the polynomial chaos framework in the following manner. Assume solution of the differential equation to be $x(t, \Delta)$. For second-order processes, the solution for every component of $x \in \mathbb{R}^n$ can be approximated as

Table 1 Correspondence between choice of polynomials and given distribution of Δ [16]

PDF of Δ	$\phi_i(\Delta)$ of the Wiener–Askey scheme
Gaussian	Hermite
Uniform	Legendre
Gamma	Laguerre
Beta	Jacobi

$$\hat{x}_i(t, \Delta) = \sum_{j=0}^{N} x_{ij}(t)\phi_j(\Delta); \qquad i = 1, \ldots, n \tag{3}$$

The above series is truncated after $N + 1$ terms, which is determined by the dimension d of Δ and the order r of the orthogonal polynomials $\{\phi_j\}$, satisfying $N + 1 = (d + r)!/d!r!$. This expression gives the number of terms in a sequence of multivariate polynomials up to order r with d variables.

Substituting the approximate solution into equation of the dynamical system results in errors, which are given by

$$e_i = \dot{\hat{x}}_i - f_i(\hat{x}, \Delta); \qquad i = 1, \ldots, n$$

The approximation in Eq. (3) is optimal in the $\mathcal{L}_2$ sense when the projection of the errors on the orthogonal basis functions are zero, i.e.,

$$\langle e_i(t, \Delta), \phi_j(\Delta)\rangle = 0 \tag{4}$$

for $j = 0, \ldots, N$; $i = 1, \ldots, n$. Equation (4) results in the following $n(N + 1)$ *deterministic* ordinary differential equations:

$$\dot{x}_{ik} = \frac{\int_{\mathcal{D}_\Delta} f(\sum_{j=0}^{N} x_{ij}(t)\phi_j(\Delta), \Delta)\phi_k(\Delta)p(\Delta)\,\mathrm{d}\Delta}{\int_{\mathcal{D}_\Delta} \phi_k^2(\Delta)p(\Delta)\,\mathrm{d}\Delta} \tag{5}$$

for $i = 1, \ldots, n$ and $k = 0, \ldots, N$. Therefore, the stochastic dynamics in $\mathbb{R}^n$ has been transformed into deterministic dynamics in $\mathbb{R}^{n(N+1)}$. Let us represent

$$X_{pc} = [\, x_{10} \cdots x_{1N} \quad x_{20} \cdots x_{2N} \quad \cdots \quad x_{n0} \cdots x_{nN} \,]^T$$

Then Eq. (5) can be written in a compact form as

$$\dot{X}_{pc} = F_{pc}(X_{pc}) \tag{6}$$

where $F_{pc}(X_{pc})$ represents the right-hand side of Eq. (5). Equation (6) can be solved using algorithms for ordinary differential equations to obtain the approximate stochastic response of the system under consideration.

This method of obtaining Eqs. (5) and (6) is referred to as the intrusive method and is difficult to compute when $f(\hat{x}, \Delta)$ is a nonpolynomial function [34]. For such cases, it is better to apply gPC on a suitable polynomial approximation of $f(\hat{x}, \Delta)$.

III. Proposed Nonlinear Estimation Scheme

Let us consider a nonlinear dynamical system being measured by a nonlinear measurement model. The states are given by $x \in \mathbb{R}^n$ and the measured outputs are $\tilde{y} \in \mathbb{R}^m$. The dynamics is governed by

$$\dot{x} = f(x, \Delta) \tag{7a}$$

$$\tilde{y} = h(x) + \nu \tag{7b}$$

where ν is the measurement noise with $\nu \sim \mathcal{N}(0, R)$. The random parameters can be written as $\Delta = [\, \Delta_{x_0} \quad \Delta_\rho \,]^T$, where Δ_{x_0} represents initial state uncertainty and Δ_ρ represents uncertainty in system parameters. Let $p(\Delta)$ be the distribution of Δ.

Estimation algorithms have essentially two steps: the propagation phase and the update phase. It is assumed that $p(\Delta)$ is stationary *during* the propagation phase. However, the distribution of $x(t, \Delta)$ will not be stationary due to the dynamics. Therefore, the distribution of Δ_{x_0} will change after every update phase. The distribution of Δ_ρ will typically not change at all, unless updated externally. Let us also assume that the measurement updates are available at discrete time $t_k, t_{k+1}, \ldots$.

A. Step 1: Initialization of State

Given the probability density function of the parameters $p^k(\Delta)$ at time t_k, the initial condition for $X_{pc}(t_k)$ at t_k can be obtained using the following equation:

$$x_{ij}(t_k) = \int_{\mathcal{D}_\Delta} \Delta_{x_{0_i}} \phi_j(\Delta) p^k(\Delta)\, \mathrm{d}\Delta \quad \text{for } i = 1, \ldots, n \quad j = 0, \ldots, N \tag{8}$$

where $\Delta_{x_0} = x(t_k, \Delta)$. The symbol $\Delta_{x_{0_i}}$ represents the ith component of Δ_{x_0}, which is the random variable associated with initial condition uncertainty.

B. Step 2: Propagation of Uncertainty and Computation of Prior Moments

With initial condition defined by Eq. (8), the system in Eq. (6) is integrated over the interval $[t_k, t_{k+1}]$ to obtain $X_{pc}(t_{k+1})$, i.e.,

$$X_{pc}(t_{k+1}) = X_{pc}(t_k) + \int_{t_k}^{t_{k+1}} F_{pc}(X_{pc}(\tau))\, \mathrm{d}\tau \tag{9}$$

The moments of the random process $x(t, \Delta)$ at $t = t_{k+1}$ can be computed from $X_{pc}(t_{k+1})$ as follows:

$$M_i^{1-} = x_{i0} \tag{10a}$$

$$M_{ij}^{2-} = \sum_{p=0}^{N} \sum_{q=0}^{N} x_{ip} x_{jq} \langle \phi_p \phi_q \rangle \tag{10b}$$

$$M_{ijk}^{3-} = \sum_{p=0}^{N} \sum_{q=0}^{N} \sum_{r=0}^{N} x_{ip} x_{jq} x_{kr} \langle \phi_p \phi_q \phi_r \rangle \tag{10c}$$

for $i, j, k = 1, \ldots, n$. The fourth and other moments can be calculated in a similar manner. Detailed derivations of the above equations, can be found in the literature [26]. Here, $x_{ij} := x_{ij}(t_{k+1})$ and M^{i-} represents the ith prior moment at t_{k+1}. The inner products of the basis functions are computed with respect to $p^k(\Delta)$, i.e.,

$$\langle \phi_p \phi_q \phi_r \phi_s \rangle = \int_{\mathcal{D}_\Delta} \phi_p(\Delta) \phi_q(\Delta) \phi_r(\Delta) \phi_s(\Delta) p^k(\Delta)\, \mathrm{d}\Delta$$

C. Step 3: Estimation of the Prior Probability Density Function from Prior Moments

When solving Eq. (9), the states $x(t_{k+1}, \Delta)$ can be approximated using Eq. (3). With this information, only the moments of the prior PDF, $p^{k+1}(\Delta)$ at time t_{k+1}, can be found [22,26]. Hence, it is difficult to estimate $p^{k+1}(\Delta)$, except when Gaussian behavior is assumed [35]. In this estimation algorithm, the prior probability density function is determined using maximum-entropy estimation theory, subject to constraints defined by the prior moments M^{i-}. This is the solution of the following optimization problem:

$$J := \max_{p^{k+1}(\Delta)} -\int_{D_\Delta} p^{k+1}(\Delta) \log(p^{k+1}(\Delta))\, \mathrm{d}\Delta \tag{11}$$

subject to

$$C_1 := \int_{D_\Delta} \Delta p^{k+1}(\Delta)\, \mathrm{d}\Delta = M^{1-} \tag{12a}$$

$$C_2 := \int_{D_\Delta} Q_2(\Delta) p^{k+1}(\Delta)\, \mathrm{d}\Delta = M^{2-} \tag{12b}$$

$$C_3 := \int_{D_\Delta} Q_3(\Delta) p^{k+1}(\Delta)\, \mathrm{d}\Delta = M^{3-} \tag{12c}$$

and so on. The symbols $Q_i(\Delta)$ are tensors of polynomials defining the moments corresponding to M^{i-}. The functional space of $p^{k+1}(\Delta)$ is approximated using Gaussian mixture models (GMMs) [36]. GMMs are dense in the space of continuous functions, and a sufficiently large mixture can exactly approximate $p^{k+1}(\Delta)$ [37]. In general, any parameterization of $p^{k+1}(\Delta)$ is possible, which will be explored in our future work. Under GMM approximation, $p^{k+1}(\Delta)$ is parameterized as

$$p^{k+1}(\Delta) = \sum_{i=1}^{M} \alpha_i \mathcal{N}(\mu_i, \Sigma_i) \tag{13}$$

with $\alpha_i \in \mathbb{R}$, $\mu_i \in \mathbb{R}^n$, $\Sigma_i = \Sigma_i^T \in \mathbb{R}^{n \times n}$, and $\Sigma_i \geq 0$. For computational simplicity, Σ_i is assumed to be diagonal, i.e., $\Sigma_i = \mathrm{diag}(\sigma_{i1} \cdots \sigma_{in})$. For $p^{k+1}(\Delta)$ to be a probability density function, the following constraint needs to be satisfied:

$$\int_{\mathcal{D}_\Delta} p^{k+1}(\Delta)\, \mathrm{d}\Delta = 1 \Rightarrow \sum_{i}^{M} \alpha_i = 1 \tag{14}$$

$$p^{k+1}(\Delta) \geq 0 \Rightarrow \alpha_i \geq 0 \tag{15}$$

Equations (14) and (15) together imply

$$0 \leq \alpha_i \leq 1 \tag{16}$$

With GMM approximation of $p^{k+1}(\Delta)$, the integrals in Eqs. (11) and (12) can be analytically computed and expressed in terms of the unknowns α_i, μ_i, and Σ_i.

Table 2 Explanation and values of the constants for Martian atmosphere [42]

Description of constants	Value
Radius of Mars	$R_m = 3397 \times 10^3$ m
Acceleration due to gravity of Mars	$g = 3.71$ m/s^2
Ballistic coefficient of the vehicle	$B_c = 72.8$ kg/m^2
Lift-to-drag ratio of the vehicle	$L/D = 0.3$
Density at the surface of Mars	$\rho_0 = 0.0019$ kg/m^3
Scale height for density computation	$h_1 = 9.8$ km $h_2 = 20$ km
Escape velocity of Mars	$v_c = 5.027$ km/s

Table 3 Scaling constants for base units

Units	Scaling constants
Mass	Mass of the vehicle is 2800 kg
Length	Radius of Mars, R_m
Time	$R_m/v_c = 675.7$ s

Table 4 Normalization factors for measurements

Measurement	Normalization factors
Dynamic pressure	1.97×10^3 N/m
Heating rate	0.0231 J/(m-s)
Flight-path angle	19.13°

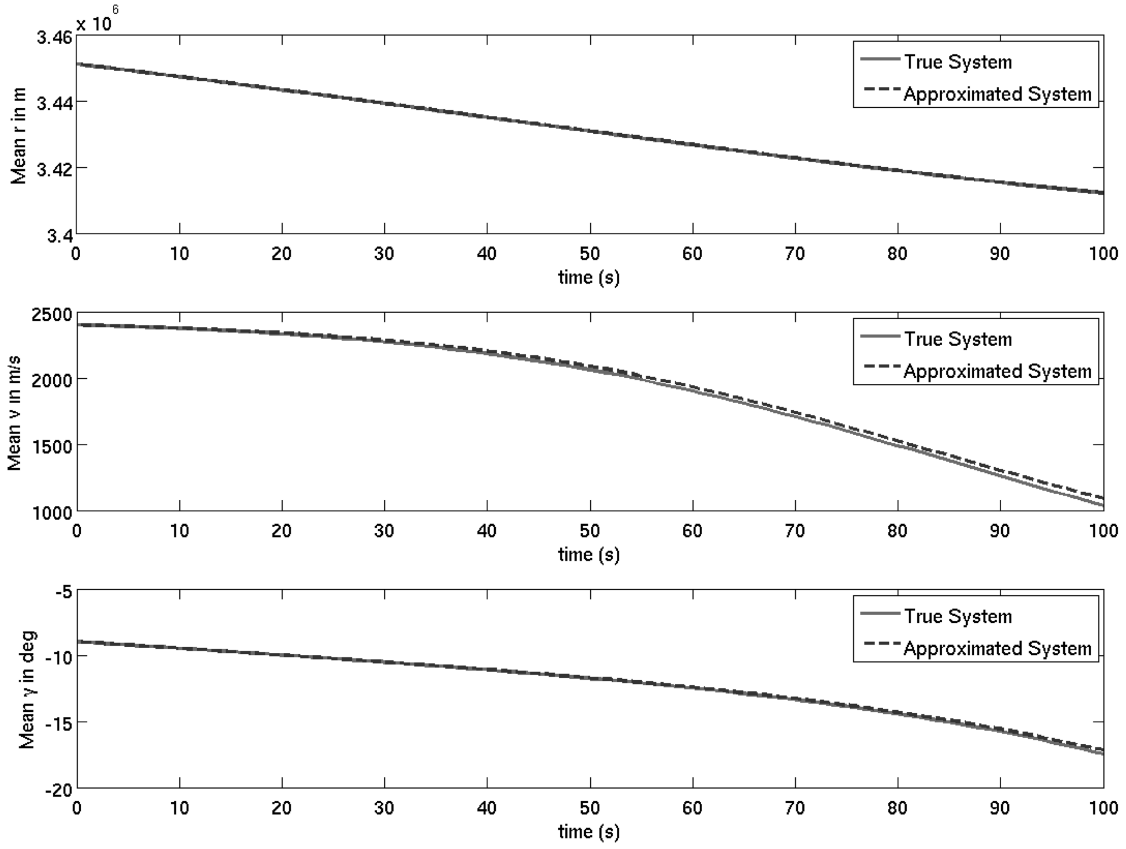

a) Mean vs. time

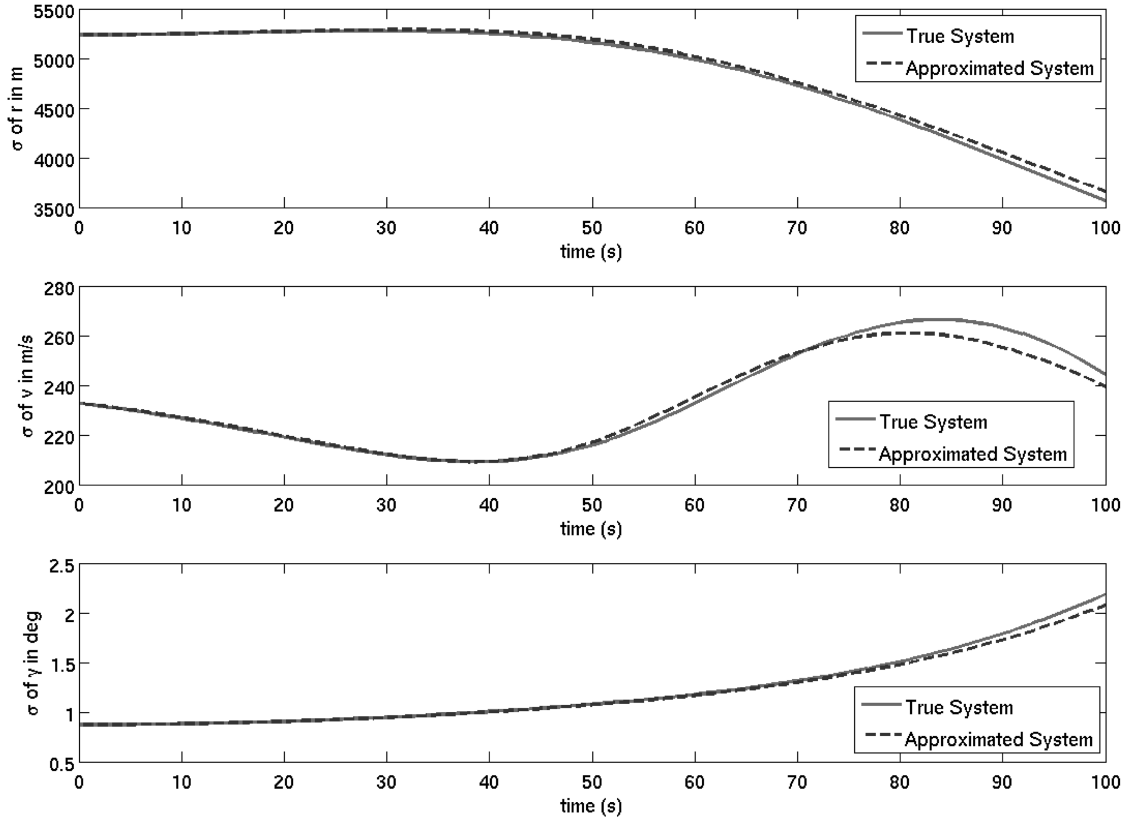

b) Standard deviation vs. time

Fig. 1 Mean and standard deviations of the true system (solid lines) and the approximated system (dashed lines) obtained from Monte Carlo simulations.

For a given term in the summation in Eq. (13) and for $x \in \mathbb{R}^3$, the cost function J_i and the constraints $C_{i,j}$ are given by the following expressions:

$$J_i = \alpha_i(\log(2) - \log(\alpha_i) + \log(\sigma_{i1}) + \log(\sigma_{i2}) + \log(\sigma_{i3}) + \log(\pi) + 1)$$

$$C_{i,1} = \mu_{i1}\alpha_i; \qquad C_{i,2} = \mu_{i2}\alpha_i; \qquad C_{i,3} = \mu_{i3}\alpha_i$$

$$C_{i,4} = \mu_{i1}^2\alpha_i + \alpha_i\sigma_{i1}^2; \qquad C_{i,5} = \mu_{i1}\mu_{i2}\alpha_i$$

$$C_{i,6} = \mu_{i2}^2\alpha_i + \alpha_i\sigma_{i2}^2; \qquad C_{i,7} = \mu_{i1}\mu_{i3}\alpha_i; \qquad C_{i,8} = \mu_{i2}\mu_{i3}\alpha_i$$

$$C_{i,9} = \mu_{i3}^2\alpha_i + \alpha_i\sigma_{i3}^2; \qquad C_{i,10} = \mu_{i1}^3\alpha_i + 3\mu_{i1}\alpha_i\sigma_{i1}^2$$

$$C_{i,11} = \mu_{i1}^2\mu_{i2}\alpha_i + \mu_{i2}\alpha_i\sigma_{i1}^2; \qquad C_{i,12} = \mu_{i1}\mu_{i2}^2\alpha_i + \mu_{i1}\alpha_i\sigma_{i2}^2$$

$$C_{i,13} = \mu_{i2}^3\alpha_i + 3\mu_{i2}\alpha_i\sigma_{i2}^2; \qquad C_{i,14} = \mu_{i3}^3\alpha_i + 3\mu_{i3}\alpha_i\sigma_{i3}^2$$

$$C_{i,15} = \mu_{i1}\mu_{i3}^2\alpha_i + \mu_{i1}\alpha_i\sigma_{i3}^2; \qquad C_{i,16} = \mu_{i2}\mu_{i3}^2\alpha_i + \mu_{i2}\alpha_i\sigma_{i3}^2$$

$$C_{i,17} = \mu_{i1}^2\mu_{i3}\alpha_i + \mu_{i3}\alpha_i\sigma_{i1}^2; \qquad C_{i,18} = \mu_{i3}\mu_{i2}^2\alpha_i + \mu_{i3}\alpha_i\sigma_{i2}^2$$

$$C_{i,19} = \mu_{i3}\mu_{i2}\mu_{i1}\alpha$$

The expressions in the above equations can also be obtained analytically for $x \in \mathbb{R}^n$. The number of constraints $C_{i,j}$ needed for $x \in \mathbb{R}^n$ is given by the following expression:

$$\dim(C_{i,j}) = \sum_{k=1}^{3} \binom{n+k-1}{k} \quad \forall\ i = 1, \ldots, M \tag{17}$$

Detailed derivation of the above formula has been omitted here and can be found in the literature [38].

If the moments are represented in column form as

$$M^{1-} = [M_1^{1-}, M_2^{1-}, M_3^{1-}]^T$$

$$M^{2-} = [M_{11}^{2-}, \ldots, M_{13}^{2-}, M_{21}^{2-}, \ldots, M_{23}^{2-}, \ldots]^T$$

$$M^{3-} = [M_{111}^{2-}, \ldots, M_{113}^{3-}, M_{121}^{3-}, \ldots, M_{123}^{3-}, M_{131}^{3-}, \ldots, M_{133}^{3-}, \ldots]^T$$

The cost J in Eq. (11) and constraints C_j in Eq. (12) are given by

$$J = \sum_{i=1}^{M} J_i; \qquad C_1 := \sum_{i=1}^{M} C_{i,j} = M_j^{1-} j = 1, \ldots, 3$$

$$C_2 := \sum_{i=1}^{M} C_{i,j} = M_{j-3}^{2-} j = 4, \ldots, 9$$

$$C_3 := \sum_{i=1}^{M} C_{i,j} = M_{j-9}^{3-} j = 10, \ldots, 19$$

It can be seen that the cost function is convex in α_i and concave in σ_{ij}. The constraints are convex in α_i and σ_{ij}, but not all the constraints are convex in μ_{ij}. The problem can be made convex by restricting $\mu_{ij} \geq 0$, which will require affine transformation of the state variables and rewriting the dynamics and output equation in terms of the new variables. The optimization problem as presented here can also be solved as a nonlinear programming problem.

D. Step 4: Parameter Estimation in Bayesian Framework

The measurements $\tilde{y}_{k+1} := \tilde{y}(t_{k+1})$ are incorporated to find the state estimate $\hat{x}_{k+1} := \hat{x}(t_{k+1})$, using the methodology given in Bryson and Ho [39]. The prior PDF used here is $p^{k+1}(\Delta)$, defined in Eq. (13). From now onward, the prior PDF will be represented as $p^{k+1-}(\Delta)$. In the Bayesian framework, first $p^{k+1}(\tilde{y}_{k+1}|\Delta = \hat{x}_{k+1})$ is calculated, which is the conditional probability density function of $\tilde{y}_{k+1}$ given the current state estimate $\hat{x}_{k+1}$. This function is called the *likelihood function*. Next, the conditional probability of the state given the current measurement $\tilde{y}_{k+1}$, i.e., $p^{k+1}(\Delta|\tilde{y}_{k+1})$, is found. The state estimate $\hat{x}_{k+1}$ is then determined using the maximum-likelihood, minimum-variance, or minimum-error criteria from $p^{k+1}(\Delta|\tilde{y}_{k+1})$.

1. *Step 4.1: Calculating the Posterior Probability Density Function*

First, the likelihood function is constructed using the Gaussian nature of measurement noise and the sensor model, as shown in Eq. (7). The likelihood function $p(\tilde{y}_{k+1}|\Delta = \hat{x}_{k+1})$ is given by

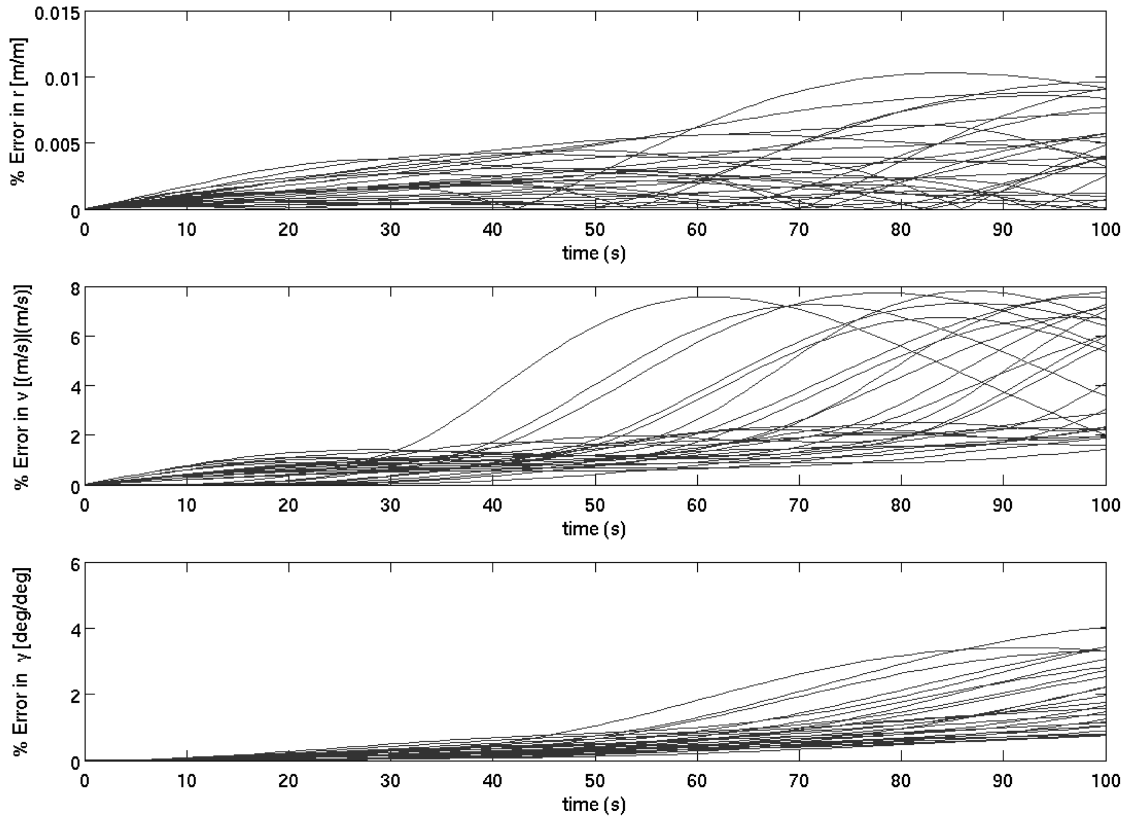

Fig. 2 Percentage error in states of the approximated system from true system.

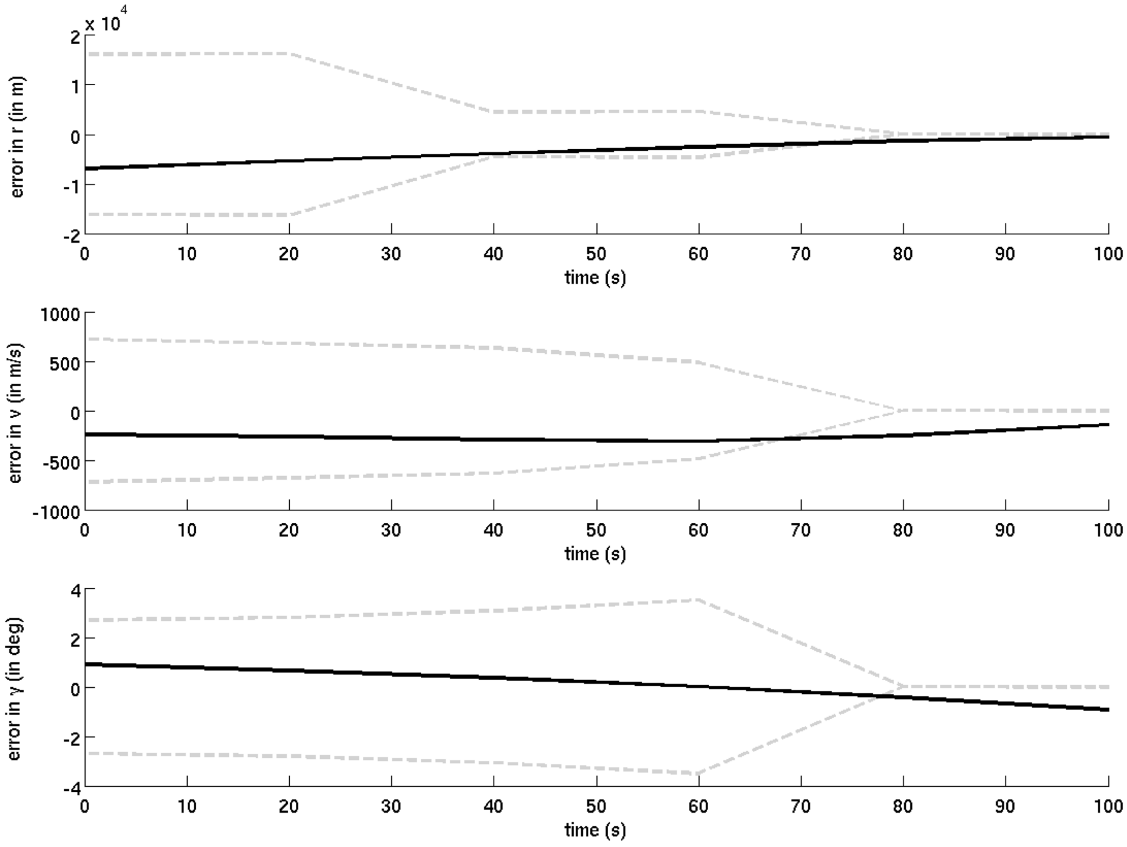

a) EKF based estimator

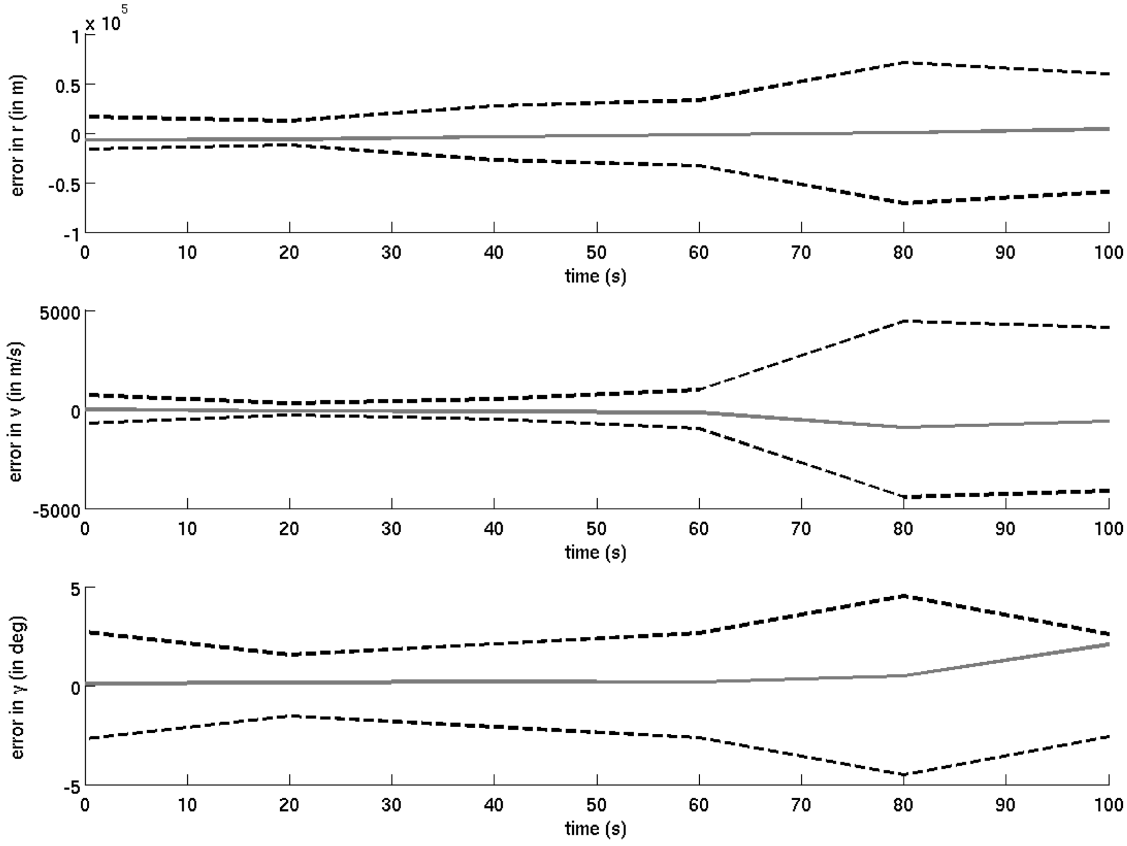

b) UKF based estimator

Fig. 3 Performances of EKF- and UKF-based estimators with true initial states as $[\,R_m + 61\ \text{km} \quad 2.42\ \text{km/s} \quad -8.91^\circ\,]^T$ and update interval of 20 s. The dashed lines represent $\pm 3\sigma$ limits and the solid line represents error in estimation.

$$p^{k+1}(\tilde{y}_{k+1}|\Delta=\hat{x}_{k+1})=\frac{1}{\sqrt{(2\pi)^m|R|}}e^{-\frac{1}{2}(\tilde{y}_{k+1}-h(\hat{x}_{k+1}))^T R^{-1}(\tilde{y}_{k+1}-h(\hat{x}_{k+1}))} \tag{18}$$

where $|R|$ is the determinant of the measurement-noise covariance matrix.

The posterior PDF is determined next, which is the density function of the states given the current measurement and is denoted by $p^{k+1}(\Delta|\tilde{y}_{k+1})$. Using the classical Bayes rule, it can be written as

$$p^{k+1}(\Delta|\tilde{y}_{k+1})=\frac{p^{k+1}(\tilde{y}_{k+1}|\Delta=\hat{x}_{k+1})p^{k+1^-}(\Delta)}{\int_{\mathcal{D}_\Delta}p^{k+1}(\tilde{y}_{k+1}|\Delta=\hat{x}_{k+1})p^{k+1^-}(\Delta)\,\mathrm{d}\Delta} \tag{19}$$

2. Step 4.2: Getting the State Estimate

Depending on the desired criterion for state estimation, the state estimate $\hat{x}_{k+1}$ is computed from $p^{k+1}(\Delta|\tilde{y}_{k+1})$. The commonly used criteria are as follows:

1) *MLE criterion*: Maximize the probability such that $\hat{x}_{k+1}=\Delta$. This is also called the most-probable estimate or maximum-likelihood estimate, which translates to

$$\hat{x}_{k+1}=\text{mode of } p^{k+1}(\Delta|\tilde{y}_{k+1})$$

2) *MCE criterion*: Minimize the covariance of $p^{k+1}(\Delta|\tilde{y}_{k+1})$, which is

$$\hat{x}_{k+1}=\min_{\Delta}\int_{\mathcal{D}_\Delta}\|\Delta-\hat{x}_{k+1}\|^2 p^{k+1}(\Delta|\tilde{y}_{k+1})\,\mathrm{d}\Delta$$

The estimate here is the mean of $p^{k+1}(\Delta|\tilde{y}_{k+1})$.

3) *MEE criterion*: Minimize maximum $|\Delta-\hat{x}_{k+1}|$, which translates to

$$\hat{x}_{k+1}=\text{median of } p^{k+1}(\Delta|\tilde{y}_{k+1})$$

E. Step 5: Generation of the Basis Functions

The posterior probability density function $p^{k+1}(\Delta|\tilde{y}_{k+1})$ becomes the density function for the initial states in the next iteration. The basis functions $\phi(\Delta)$ are generated such that they are orthogonal to each other with respect to new probability density function. If $\{\phi_i(\Delta)\}$ are orthogonal, the gPC approximations have exponential convergence and are thus optimal. For any other basis functions, the approximation is worse than optimal. However, for some applications, use of the same basis functions for all the time steps may provide acceptable results. The Gram–Schmidt procedure, similar to Eq. (2), is used to generate the set of basis functions $\{\phi_i(\Delta)\}$ that are orthogonal. Consequently, all the inner products in the estimation algorithm presented need to be recomputed at every time step.

Analytical computation of the basis functions using Gram–Schmidt procedure is tedious and increases in complexity as the number of states increase [40]. To avoid this, the domain $\mathcal{D}_\Delta$ of Δ is discretized and the basis function values are numerically calculated at each grid point of the discretized domain. The required integrations are performed numerically for univariate polynomials, which can be computed efficiently. Polyvariate polynomials are then determined using tensor products of the univariate polynomials.

IV. Application to Hypersonic Reentry Problem

The estimation algorithm presented here is applied to reentry of hypersonic vehicles. The simplified dynamics of reentry are represented by Vinh's equation [41] in three states: the distance from the planet's center r, velocity v, and the flight-path angle γ, or $x=[\,r\quad v\quad \gamma\,]^T$. The equations can be written as

$$\dot{r}=v\sin(\gamma) \tag{20a}$$

$$\dot{v}=-\frac{\rho v^2}{2B_c}-g\sin(\gamma) \tag{20b}$$

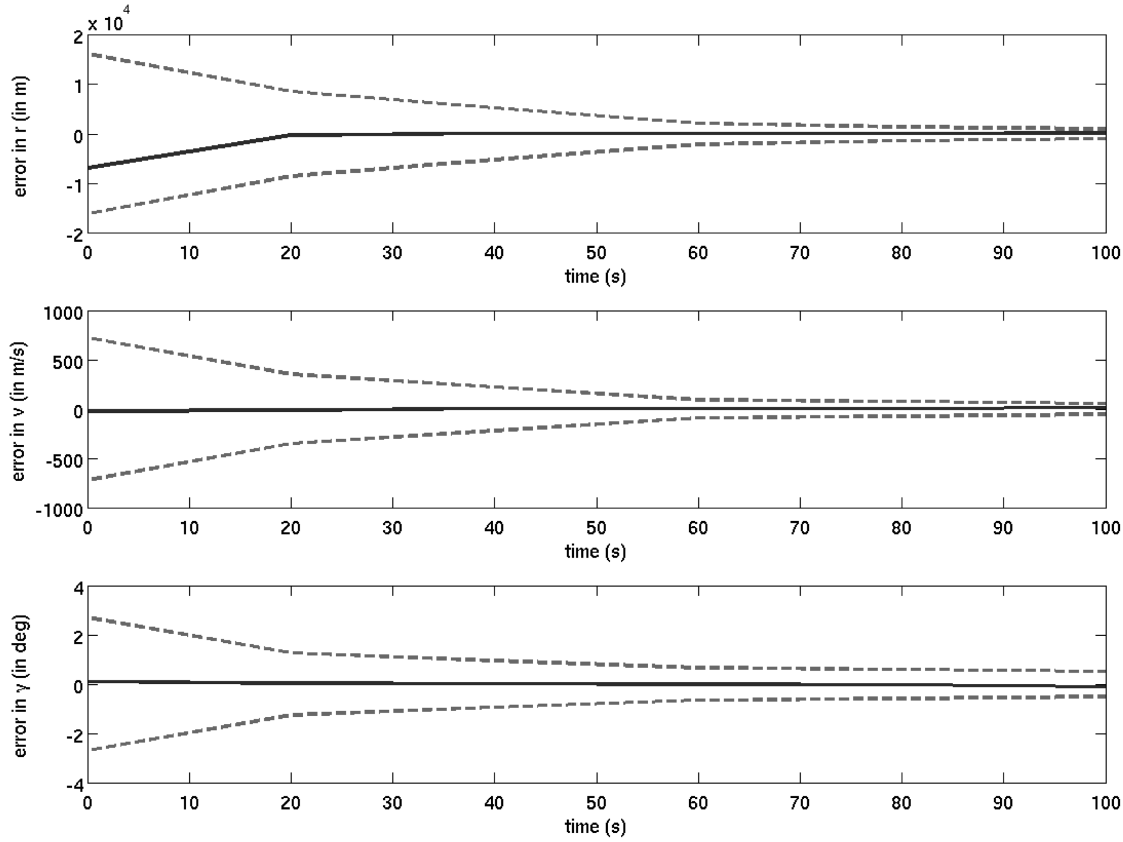

Fig. 4 Performance of the gPC-based estimator with true initial states as $[\,R_m+61\ \text{km}\quad 2.42\ \text{km/s}\quad -8.91^\circ\,]^T$ and update interval of 20 s. The dashed lines represent $\pm 3\sigma$ limits and the solid line represents error in estimation.

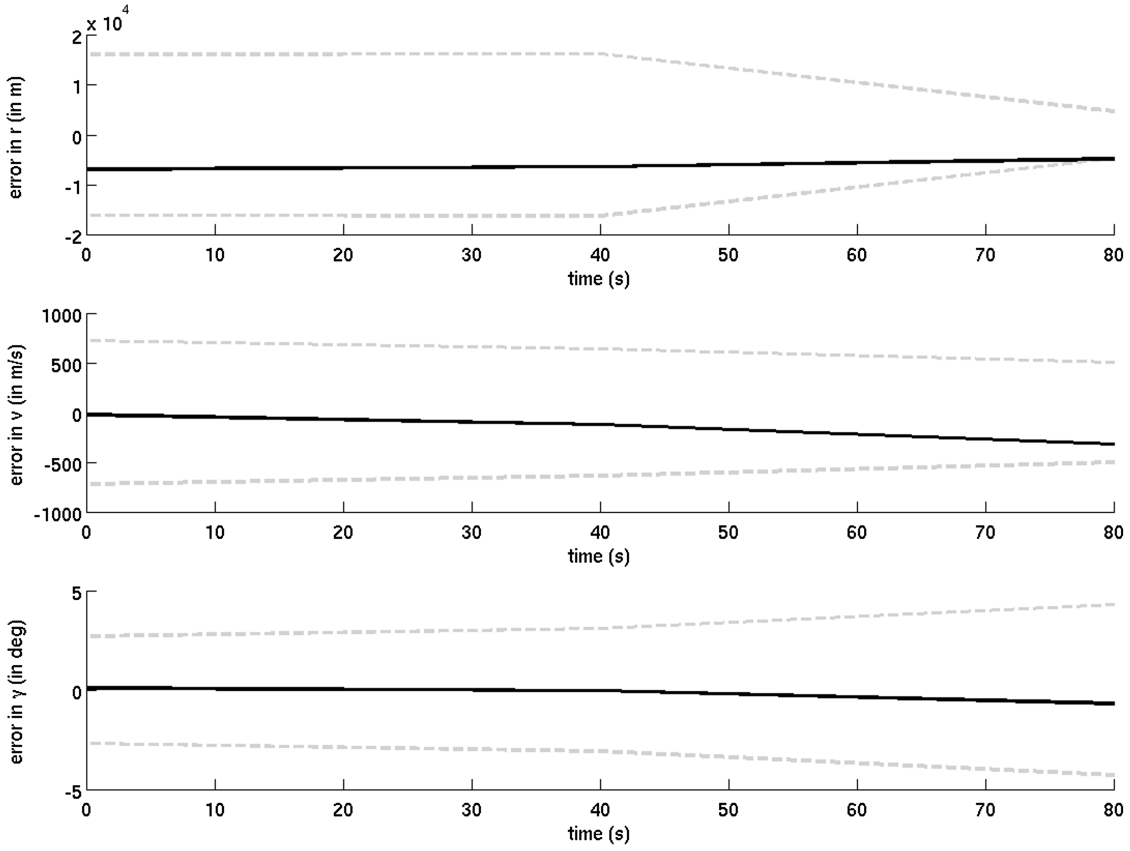

a) EKF based estimator

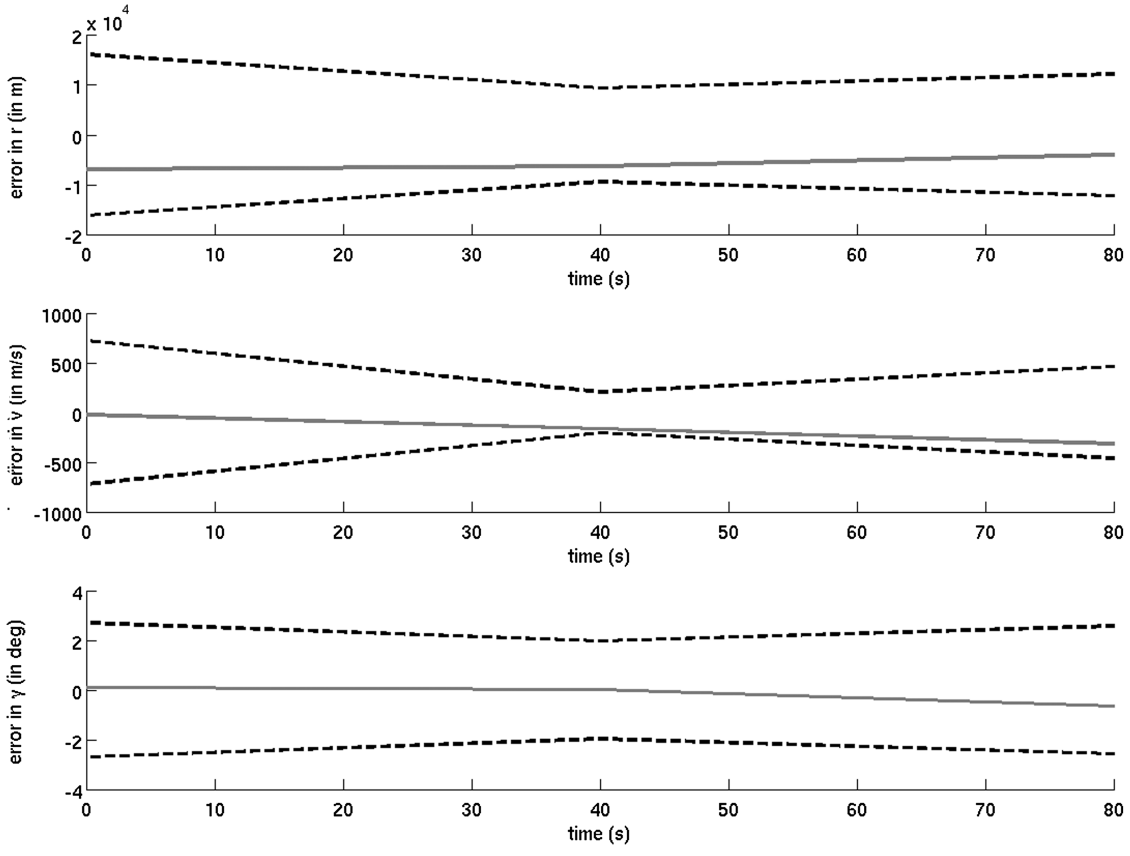

b) UKF based estimator

Fig. 5 Performances of EKF- and UKF-based estimator with true initial states as $[\,R_m + 61\ \text{km} \quad 2.42\ \text{km/s} \quad -8.91^\circ\,]^T$ and update interval of 40 s. The dashed lines represent $\pm 3\sigma$ limits and the solid line represents error in estimation.

$$\dot{\gamma} = \left(\frac{v}{r} - \frac{g}{v}\right)\cos(\gamma) + \frac{1}{2B_c}\left(\frac{L}{D}\right)v \tag{20c}$$

where g is the acceleration due to gravity, B_c is the ballistic coefficient, L/D is the lift-to-drag ratio of the vehicle, and ρ is the atmospheric density given by

$$\rho = \rho_0 e^{\left(\frac{h_2 - h}{h_1}\right)}$$

where ρ_0, h_1, and h_2 are constants depending on the planet's atmospheric model; $h = r - R_m$ is the height above the planet's surface; and R_m is the radius of the planet. Choices of the constants in Eq. (20) used to simulate reentry in Martian atmosphere are given in Table 2.

The measurement model $\tilde{y}$ consists of the dynamic pressure $\bar{q}$, the heating rate Q [43], and the flight-path angle, or $\tilde{y} = [\,\bar{q} \quad Q \quad G\,]^T$, where the expressions are

$$\bar{q} = \tfrac{1}{2}\rho v^2 \tag{21a}$$

$$Q = k\rho^{\frac{1}{2}}v^{3.15} \tag{21b}$$

$$G = \gamma \tag{21c}$$

where $k = 4.47228 \times 10^{-9}$ is the scaled material heating coefficient.

Here, initial state uncertainty with Gaussian distribution has been considered, i.e., $x(0, \Delta) = \Delta \sim \mathcal{N}(\mu_0, \sigma_0^2)$, where μ_0 and σ_0 are mean and standard deviations, respectively, and have the values

$$\mu_0 = [\,R_m + 54 \text{ km}, \quad 2.4 \text{ km/s}, \quad -9^\circ\,]^T \tag{22a}$$

$$\sigma_0 = \begin{pmatrix} 5.4 \text{ km} & 0 & 0 \\ 0 & 240 \text{ m/s} & 0 \\ 0 & 0 & 0.9^\circ \end{pmatrix} \tag{22b}$$

To achieve consistency in dimensions, every constant in Eq. (20) is scaled appropriately to create a nondimensionalized system. The constants scaling the base units are given in Table 3.

The measurements are normalized to lie within $[-1, 1]$ so that they have consistent magnitude. The normalization factors used for measurements are given in Table 4. The measurement noise ν is assumed to have mean and covariance of $\mathbf{E}[\nu] = [\,0, \quad 0, \quad 0\,]^T$ and $R = \mathbf{E}[\nu\nu^T] = 6 \times 10^{-5}\mathcal{I}_3$, respectively.

As mentioned before, gPC theory works best when the nonlinearities are in the form of polynomials [34,44]. In this case, the trigonometric and exponential terms in Eq. (20) are approximated, with cubic polynomials in γ and h, respectively. For example, let $S(\gamma)$ be a suitable approximation of $\sin(\gamma)$, then

$$S(\gamma) = a_0 + a_1\gamma + a_2\gamma^2 + a_3\gamma^3$$

and

$$S'(\gamma) = a_1 + 2a_2\gamma + 3a_3\gamma^2$$

The coefficients of $S(\gamma)$ are obtained by equating the values of $\sin(\gamma)$ and its derivative, with $S(\gamma)$ and $S'(\gamma)$, respectively, at the boundaries of the γ domain. For the present case, $\gamma \in [-90^\circ, 0]$, which yields a system of linear equations given by

$$\begin{pmatrix} 1 & -1.57 & 2.47 & -3.88 \\ 1 & 0 & 0 & 0 \\ 0 & 1 & -3.14 & 7.40 \\ 0 & 1 & 0 & 0 \end{pmatrix}\begin{pmatrix} a_0 \\ a_1 \\ a_2 \\ a_3 \end{pmatrix} = \begin{pmatrix} -1 \\ 0 \\ 0 \\ 1 \end{pmatrix}$$

which can be solved for a_0, a_1, a_2, and a_3. The approximation of $\cos(\gamma)$ can be found in a similar manner.

The approximation of sine and cosine terms for the present case are

$$\sin(\gamma) \approx S(\gamma) := \gamma + 0.0574\gamma^2 - 0.1107\gamma^3$$

$$\cos(\gamma) \approx C(\gamma) := 1 - 0.5792\gamma^2 - 0.1107\gamma^3$$

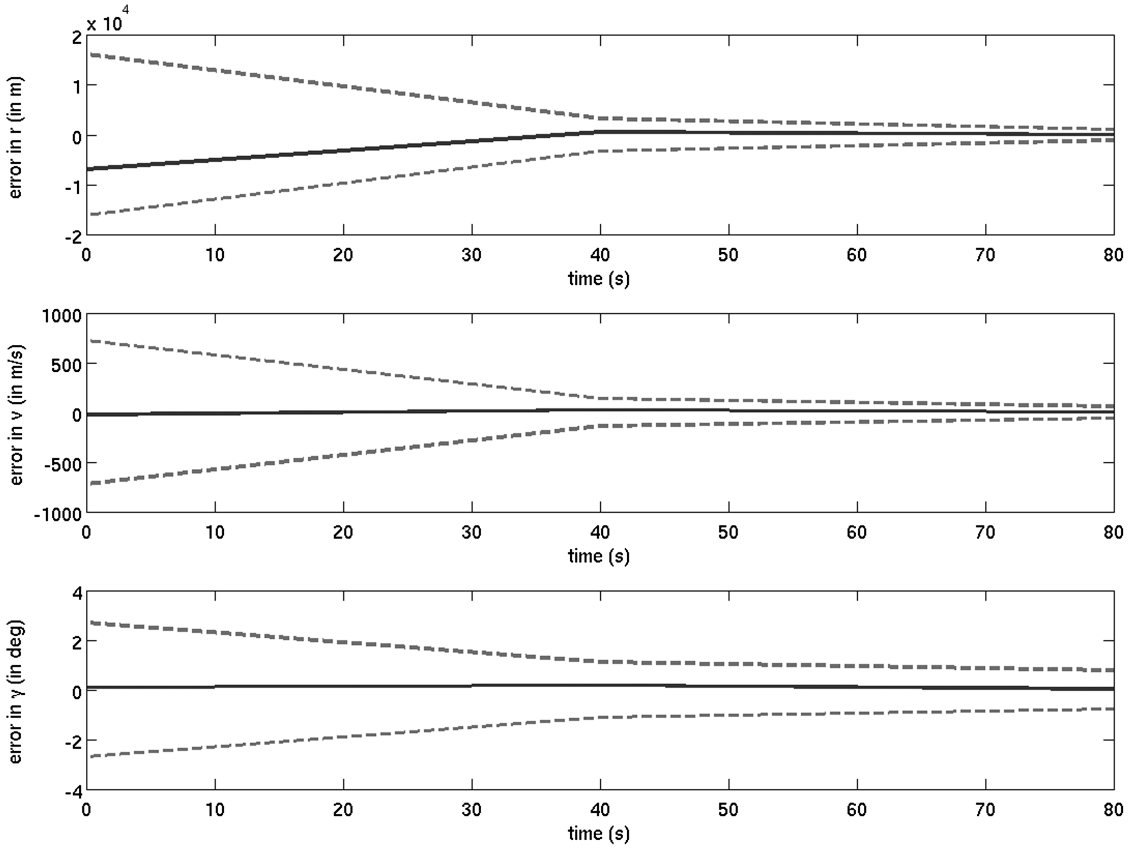

Fig. 6 Performance of the gPC-based estimator with true initial states as $[\,R_m + 61 \text{ km} \quad 2.42 \text{ km/s} \quad -8.91^\circ\,]^T$ and update interval of 40 s. The dashed lines represent $\pm 3\sigma$ limits and the solid line represents error in estimation.

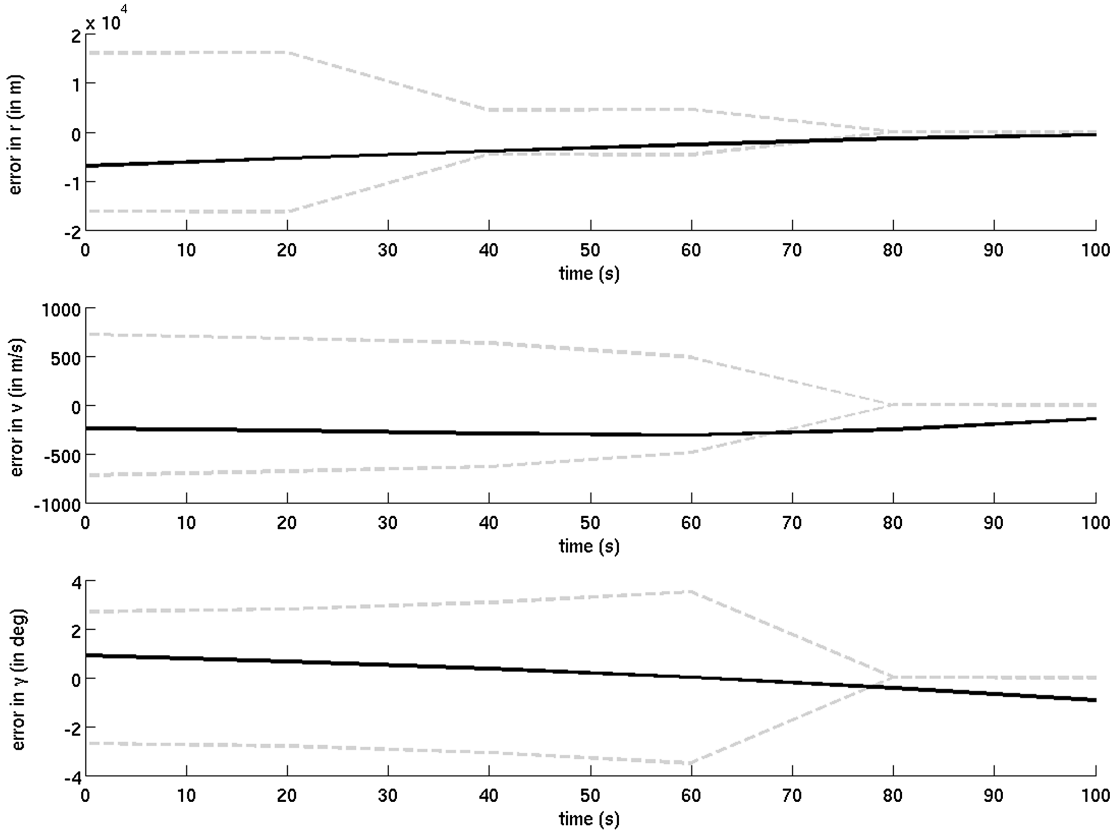

a) EKF based estimator

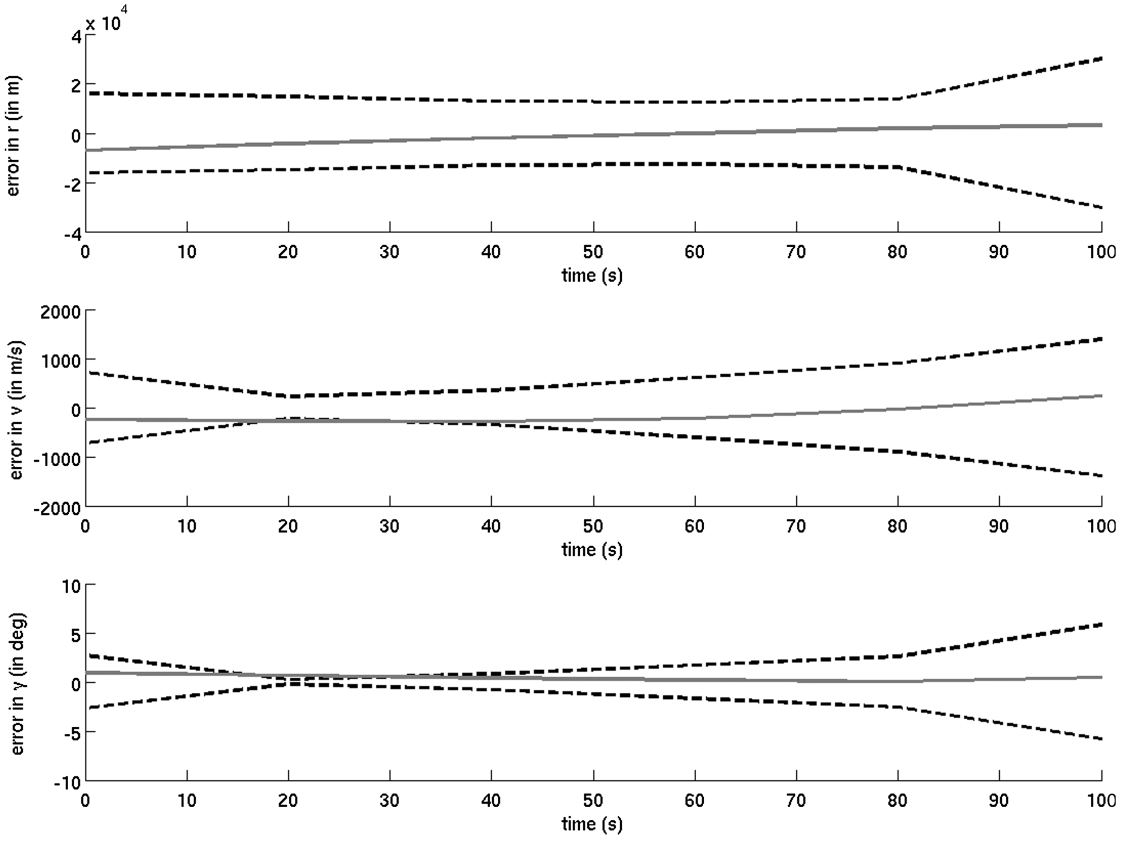

b) UKF based estimator

Fig. 7 Performance of EKF- and UKF-based estimators with true initial states as $[R_m + 61\ \text{km} \quad 2.64\ \text{km/s} \quad -8.1^\circ]^T$ and update interval of 20 s. The dashed lines represent $\pm 3\sigma$ limits and the solid line represents error in estimation.

Assuming $h \in [0, 100\text{ km}]$, the exponential density term is approximated by cubic polynomials in three different intervals. The approximated density term $D(h)$ is given by

$$\rho \approx D(h) := \begin{cases} 0.0146 - 1.50 \times 10^{-6}h + 5.93 \times 10^{-11}h^2 - 8.45 \times 10^{-16}h^3 & 0 \le h < 25\text{ km} \\ 0.0080 - 4.72 \times 10^{-7}h + 9.59 \times 10^{-12}h^2 - 6.61 \times 10^{-17}h^3 & 25\text{ km} \le h < 50\text{ km} \\ 0.0015 - 5.2 \times 10^{-8}h + 5.90 \times 10^{-13}h^2 - 2.20 \times 10^{-18}h^3 & 50\text{ km} \le h < 100\text{ km} \end{cases}$$

The approximated system can be written as

$$\dot{r} = vS(\gamma) \tag{23a}$$

$$\dot{v} = -\frac{D(h)v^2}{2B_c} - gS(\gamma) \tag{23b}$$

$$\dot{\gamma} = \left(\frac{v}{r} - \frac{g}{v}\right)C(\gamma) + \frac{1}{2B_c}\left(\frac{L}{D}\right)v \tag{23c}$$

Monte Carlo simulations were performed to validate the approximated model. A Gaussian distribution for initial states was assumed, with mean and standard deviations as given in Eq. (22). Figure 1 shows the trajectories of mean and the standard deviations for systems in Eqs. (20) and (23). It can be seen that they are almost identical for both the systems, although some variation is observed for longer propagation time. Figure 2 shows the percentage error in approximation of the systems' states. From this analysis it can be concluded that the system in Eq. (23) is a good approximation of the actual system in Eq. (20) for estimation purposes. Clearly, a better approximation could be performed that reduces the growth of error over long time integration. However, with this model, good results were obtained for the estimation algorithm. The approximated model is used to propagate the uncertainty. The measurements were obtained by simulating the actual nonlinear system.

To construct the deterministic dynamical system via polynomial chaos as defined in Eq. (6), inner products of up to six basis functions were required. Detailed derivation of the augmented dynamics has been omitted from this paper and can be found in Prabhakar et al. [44].

Up to fourth-order moments were used to compute the prior probability density function from GMMs. The prior moments M^{i-} for $i = 1, \ldots, 4$ were computed from the gPC coefficients X_{PC} and the inner products $\langle \phi_i \phi_j \ldots \rangle$, as in Eq. (10). In this example, the associated optimization problem has been solved as a nonlinear programming problem (NLP), using SNOPT [45]. Clearly, there are issues related to convergence of this optimization problem. In the simulations, the NLP converged to a local solution at every time step. There are methods to convert this optimization problem to a convex optimization problem, and they will be considered in our future work.

The performance of the proposed estimator was then compared with EKF- and UKF-based estimators. For the current analysis, the covariance of the posterior PDF was minimized to get the state estimate (MCE criterion), which is the mean of the posterior density function. The initial states of the true system were assumed to be

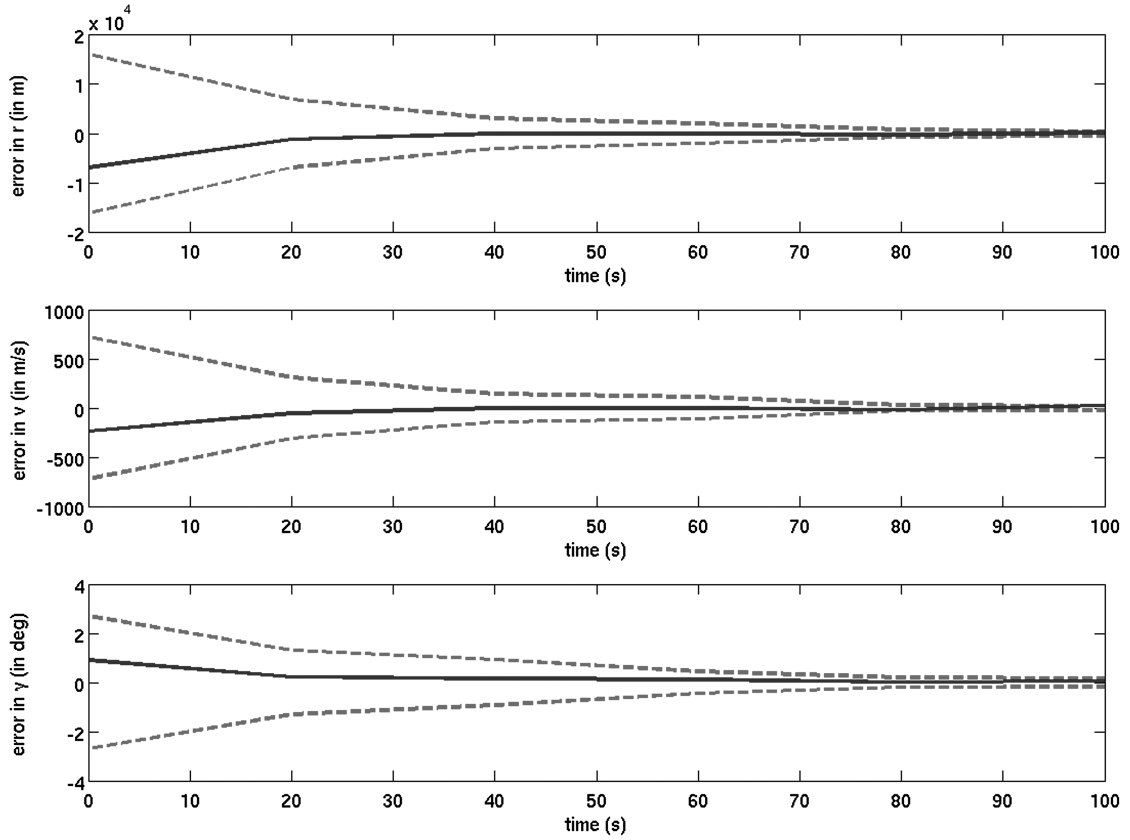

Fig. 8 Performance of the gPC-based estimator with true initial states as $[R_m + 61\text{ km} \quad 2.64\text{ km/s} \quad -8.1^\circ]^T$ and update interval of 20 s. The dashed lines represent $\pm 3\sigma$ limits and the solid line represents error in estimation.

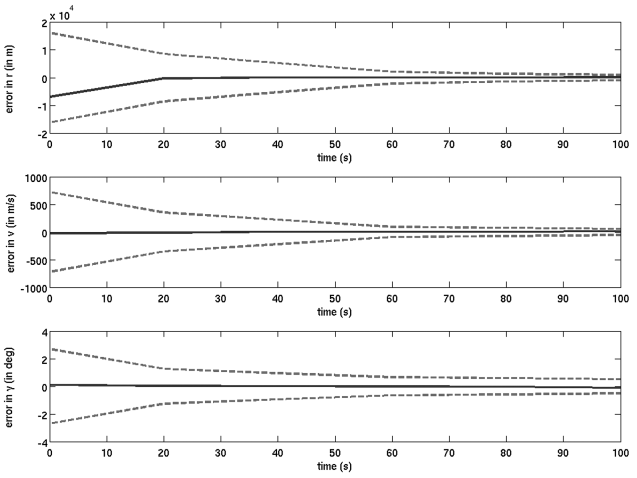

a) MCE criterion

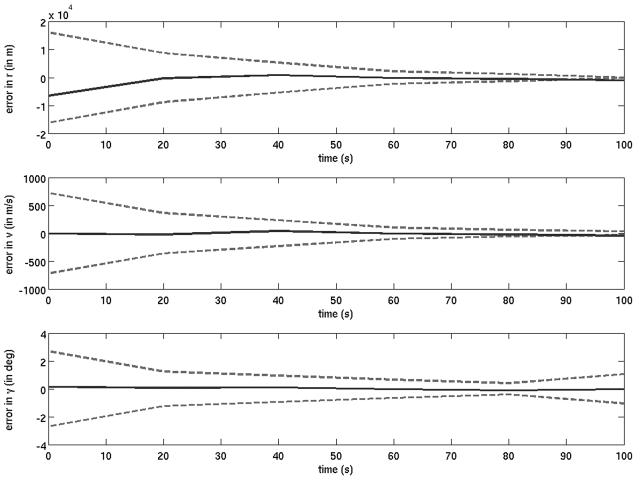

b) MLE criterion

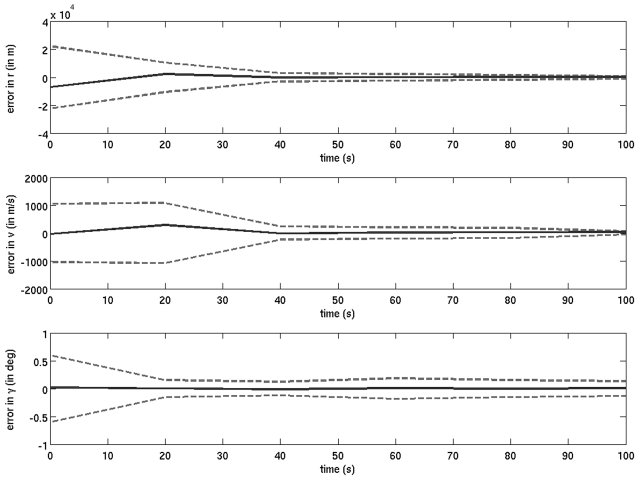

c) MEE criterion

Fig. 9 Performances of MCE, MLE, and MEE criteria for state estimates. The true initial states are $[\,R_m + 61\ \text{km} \quad 2.42\ \text{km/s} \quad -8.91^\circ\,]^T$ and update interval is 20 s. The dashed lines represent $\pm 3\sigma$ limits and the solid line represents error in estimation.

$$x(t=0) = [\,R_m + 61\ \text{km} \quad 2.42\ \text{km/s} \quad -8.91^\circ\,]^T$$

Therefore, the initial error in state estimation was $[-7\ \text{km} \quad -0.02\ \text{km/s} 0.09^\circ]^T$. Figures 3 and 4, shows the plots for error in state estimation, where the measurement update interval is 20 s. It can be observed that the errors for gPC-based estimator goes to zero rapidly and are within the $\pm 3\sigma$ limits. The EKF-based estimator performs poorly and the errors do not converge to zero. The EKF-based estimator is also inconsistent, as the errors escape outside $\pm 3\sigma$ limits. In case of UKF, the errors for γ and v starts to increase after a while and the $\pm 3\sigma$ limits are divergent. In Figs. 5 and 6 the update interval was increased to 40 s. It can be seen that the errors and the $\pm 3\sigma$ bounds for the gPC-based estimator converge. The errors for the EKF-based estimator for this case diverge. Although the $\pm 3\sigma$ limits of the UKF-based estimator converge, the convergence is slower than those of the gPC-based estimator. The estimation errors for UKFs are divergent.

The gPC-based estimator works well even for larger errors in initial state estimation. For plots in Figs. 7 and 8, the true initial states were $[\,R_m + 61\ \text{km} \quad 2.64\ \text{km/s} \quad -8.1^\circ\,]^T$, with v and γ having 10% errors in initial estimate. It can be observed that gPC-based estimator achieves convergence of error and remains within $\pm 3\sigma$ bounds. For EKF, the errors diverge and escape outside the $\pm 3\sigma$ limits. Hence, the EKF-based estimator here is inconsistent. The errors for the UKF-based estimator converge but briefly remain outside the $\pm 3\sigma$ bounds. For this example, the $\pm 3\sigma$ limits for UKFs are observed to be divergent. This highlights the advantage of using polynomial chaos for propagation in Bayesian estimation framework over traditional filters based on Gaussian theory.

Figure 9 compares the performances of the three criteria functions used to get the state estimate. It is observed that $\pm 3\sigma$ bounds of MEE criterion converge faster than MCE and MLE criteria, although the bounds for MLE-based estimate diverge toward the end. The error convergence for MEE is slower than that MCE and MLE, but errors are within $\pm 3\sigma$ limits for all the criteria. When compared with EKF and UKF, the gPC-based estimators outperform both of them when convergence of errors and $\pm 3\sigma$ limits are considered.

V. Conclusions

This paper presents a nonlinear estimation algorithm that combines generalized polynomial chaos with Bayesian estimation. The estimation algorithm was applied to hypersonic reentry of a vehicle in Mars' atmosphere using three criteria for estimation (MEE, MCE, and MLE). The results obtained were compared with EKF- and UKF-based estimators. It was observed that the estimation algorithm presented here outperforms EKF and UKF for the current application. This highlights the advantage of the proposed estimator over EKF- and UKF-based estimators for systems with high nonlinearities and sparse measurements. Future plans are to compare the gPC-based estimator with particle filters and other nonlinear filtering techniques with non-Gaussian assumptions on a few benchmark problems.

Acknowledgments

This research work was conducted under NASA funding from NRA NNH06ZEA001N-HYP, under cooperative agreement number NNX07AC44A, Fundamental Aeronautics: Hypersonics Project, Topic 5.4 Advanced Control Methods, Subtopic A.5.4.1 Advanced Adaptive Control, with Dan Moerder from NASA Langley Research Center as the Technical Monitor.

References

[1] Kalman, R. E., "A New Approach to Linear Filtering and Prediction Problems," *Journal of Basic Engineering*, Vol. 82, No. 1, 1960, pp. 35–45.

[2] Anderson, B., Moore, J. B., and Eslami, M., "Optimal Filtering," *IEEE Transactions on Systems, Man, and Cybernetics*, Vol. 12, No. 2, 1982, pp. 235–236.
doi:10.1109/TSMC.1982.4308806

[3] Welch, G., and Bishop, G., *An Introduction to the Kalman Filter*, Univ. of North Carolina at Chapel Hill, Chapel Hill, NC, 1995.

[4] Evensen, G., "Using the Extended Kalman Filter with a Multilayer Quasi-Geostrophic Ocean Model," *Journal of Geophysical Research*, Vol. 97, No. C11, 1992, pp. 17905–17924.
doi:10.1029/92JC01972

[5] Miller, R. N., Ghil, M., and Gauthiez, F., "Advanced Data Assimilation in Strongly Nonlinear Dynamical Systems," *Journal of the Atmospheric Sciences*, Vol. 51, No. 8, 1994, pp. 1037–1056.
doi:10.1175/1520-0469(1994)051<1037:ADAISN>2.0.CO;2

[6] Gauthier, P., Courtier, P., and Moll, P., "Assimilation of Simulated Wind Lidar Data with a Kalman Filter," *Monthly Weather Review*, Vol. 121, No. 6, 1993, pp. 1803–1820.
doi:10.1175/1520-0493(1993)121<1803:AOSWLD>2.0.CO;2

[7] Bouttier, F., "A Dynamical Estimation of Forecast Error Covariances in an Assimilation System," *Monthly Weather Review*, Vol. 122, No. 10, 1994, pp. 2376–2390.
doi:10.1175/1520-0493(1994)122<2376:ADEOFE>2.0.CO;2

[8] Julier, S., Uhlmann, J., Durrant-Whyte, H. F., Ind, I., and City, J., "A New Method for the Nonlinear Transformation of Means and Covariances in Filters and Estimators," *IEEE Transactions on Automatic Control*, Vol. 45, No. 3, 2000, pp. 477–482.
doi:10.1109/9.847726

[9] Tanizaki, H., *Nonlinear Filters: Estimation and Applications*, Springer–Verlag, New York, 1996.

[10] Doucet, A., Godsill, S., and Andrieu, C., "On Sequential Monte Carlo Sampling Methods for Bayesian Filtering," *Statistics and Computing*, Vol. 10, No. 3, 2000, pp. 197–208.
doi:10.1023/A:1008935410038

[11] Doucet, A., de Freitas N., and Gordon, N., "An Introduction to Sequential Monte Carlo Methods," *Sequential Monte Carlo Methods in Practice*, Springer, New York, 2001, pp. 3–14.

[12] Gordon, N. J., Salmond, D. J., and Smith, A. F. M., "Novel Approach to Nonlinear/Non-Gaussian Bayesian State Estimation," *IEE Proceedings F, Radar and Signal Processing*, Vol. 140, 1993, pp. 107–113.

[13] Arulampalam, M. S., Maskell, S., Gordon, N., Clapp, T., Sci, D., Organ, T., and Adelaide, S. A., "A Tutorial on Particle Filters for Online Nonlinear/Non-Debs-Gaussian Bayesian Tracking," *IEEE Transactions on Signal Processing*, Vol. 50, No. 2, 2002, pp. 174–188.
doi:10.1109/78.978374

[14] Ristic, B., Arulampalam, S., and Gordon, N., *Beyond The Kalman Filter: Particle Filters for Tracking Applications*, Artech House, Boston, 2004.

[15] Snyder, C., Bengtsson, T., Bickel, P., and Anderson, J., "Obstacles to High-Dimensional Particle Filtering," *Monthly Weather Review*, Vol. 136, No. 12, 2008, pp. 4629–4640.
doi:10.1175/2008MWR2529.1

[16] Xiu, D., and Karniadakis, G. E., "The Wiener—Askey Polynomial Chaos for Stochastic Differential Equations," *SIAM Journal on Scientific Computing*, Vol. 24, No. 2, 2002, pp. 619–644.
doi:10.1137/S1064827501387826

[17] Wiener, N., "The Homogeneous Chaos," *American Journal of Mathematics*, Vol. 60, No. 4, 1938, pp. 897–936.
doi:10.2307/2371268

[18] Cameron, R. H., and Martin, W. T., "The Orthogonal Development of Non-Linear Functionals in Series of Fourier-Hermite Functionals," *Annals of Mathematics*, Vol. 48, No. 2, 1947, pp. 385–392.
doi:10.2307/1969178

[19] Askey, R., and Wilson, J., "Some Basic Hypergeometric Polynomials that Generalize Jacobi Polynomials," *Memoirs of the American Mathematical Society*, Vol. 54, No. 319, March 1985.

[20] Hou, T. Y., Luo, W., Rozovskii, B., and Zhou, H. M., "Wiener Chaos Expansions and Numerical Solutions of Randomly Forced Equations of Fluid Mechanics," *Journal of Computational Physics*, Vol. 216, No. 2, 2006, pp. 687–706.
doi:10.1016/j.jcp.2006.01.008

[21] Xiu, D., and Karniadakis, G. E., "Modeling Uncertainty in Flow Simulations via Generalized Polynomial Chaos," *Journal of Computational Physics*, Vol. 187, No. 1, 2003, pp. 137–167.
doi:10.1016/S0021-9991(03)00092-5

[22] Ghanem, R. G., and Spanos, P. D., *Stochastic Finite Elements: A Spectral Approach*, Springer–Verlag, New York, 1991.

[23] Ghanem, R., and Red-Horse, J., "Propagation of Probabilistic Uncertainty in Complex Physical Systems Using a Stochastic Finite Element Approach," *Physica D*, Vol. 133, No. 1-4, 1999, pp. 137–144.
doi:10.1016/S0167-2789(99)00102-5

[24] Ghanem, R. G., "Ingredients for a General Purpose Stochastic Finite Elements Implementation," *Computer Methods in Applied Mechanics and Engineering*, Vol. 168, Nos. 1–4, 1999, pp. 19–34.
doi:10.1016/S0045-7825(98)00106-6

[25] Fisher, J., and Bhattacharya, R., "Optimal Trajectory Generation with Probabilistic System Uncertainty Using Polynomial Chaos," *Journal of Dynamic Systems, Measurement, and Control* (to be published).

[26] Fisher, J., and Bhattacharya, R., "Linear Quadratic Regulation of Systems with Stochastic Parameter Uncertainties," *Automatica*, Vol. 45, No. 12, Dec. 2009, pp. 2831–2841.
doi:10.1016/j.automatica.2009.10.001

[27] Fisher, J., and Bhattacharya, R., "Stability Analysis of Stochastic Systems Using Polynomial Chaos," *American Control Conference*, Inst. of Electrical and Electronics Engineers, Piscataway, NJ, 2008, pp. 4250–4255.

[28] Nagy, Z. K., and Braatz, R. D., "Robust Nonlinear Model Predictive Control of Batch Processes," *AIChE Journal*, Vol. 49, No. 7, 2003, pp. 1776–1786.
doi:10.1002/aic.690490715

[29] Nagy, Z. K., and Braatz, R. D., "Open-Loop and Closed-Loop Robust Optimal Control of Batch Processes Using Distributional and Worst-Case Analysis," *Journal of Process Control*, Vol. 14, No. 4, 2004, pp. 411–422.
doi:10.1016/j.jprocont.2003.07.004

[30] Hover, F. S., and Triantafyllou, M. S., "Application of Polynomial Chaos in Stability and Control," *Automatica*, Vol. 42, No. 5, 2006, pp. 789–795.
doi:10.1016/j.automatica.2006.01.010

[31] Sandu, C., Blanchard, E. D., Sandhu, A., "A Polynomial Chaos Based Bayesian Approach for Estimating Uncertain Parameters of Mechanical Systems Part 1: Theoretical Approach," Computer Science Dept., Virginia Polytechnic Inst. and State Univ., TR-07-38, Blacksburg, VA, 2007.

[32] Sandu, C., Blanchard, E. D., Sandhu, A., "A Polynomial Chaos Based Bayesian Approach for Estimating Uncertain Parameters of Mechanical Systems Part 1: Theoretical Approach," Computer Science Dept., Virginia Polytechnic Inst. and State Univ., TR-07-39, Blacksburg, VA, 2007.

[33] Arfken, G. B., Arfken, G. B., and Weber, H. J., *Mathematical Methods for Physicists*, Academic Press, New York, 2001.

[34] Debusschere, B. J., Najm, H. N., Pébay, P. P., Knio, O. M., Ghanem, R. G., and Le Maître, O. P., "Numerical Challenges in the Use of Polynomial Chaos Representations for Stochastic Processes," *SIAM Journal on Scientific Computing*, Vol. 26, No. 2, 2004, pp. 698–719.
doi:10.1137/S1064827503427741

[35] Casella, G., Berger, R. L., and Berger, R. L., *Statistical Inference*, Duxbury, Pacific Grove, CA, 2002.

[36] Rasmussen, C. E., "The Infinite Gaussian Mixture Model," *Advances in Neural Information Processing Systems*, Vol. 12, MIT Press, Cambridge, MA, 2000, pp. 554–560.

[37] Ripley, B. D., *Pattern Recognition and Neural Networks*, Cambridge Univ. Press, New York, 2008.

[38] Bourbaki, N., *Elements of Mathematics. Commutative Algebra*, Springer–Verlag, ,New York, 1998, Chaps. 1–7.

[39] Bryson, A. E., and Ho, Y. C., *Applied Optimal Control: Optimization, Estimation, and Control*, Taylor & Francis, London, 1975.

[40] Möller, R., "First-Order Approximation of Gram-Schmidt Orthonormalization Beats Deflation in Coupled PCA Learning Rules," *Neurocomputing: Variable Star Bulletin*, Vol. 69, Nos. 13–15, 2006, pp. 1582–1590.

doi:10.1016/j.neucom.2005.06.016
[41] Chern, J.-S., and Vinh, N. X., "Optimal Reentry Trajectories of a Lifting Vehicle," NASA CR-3236, 1980.
[42] Sengupta, P., and Bhattacharya, R., "Uncertainty Analysis of Hypersonic Flight Using Multi-Resolution Markov Operators," AIAA Guidance, Navigation, and Control Conference and Exhibit, Honolulu, HI, AIAA Paper 2008-6298, 2008.
[43] Bollino, K. P., Ross, I. M., and Doman, D. D., "Optimal Nonlinear Feedback Guidance for Reentry Vehicles," AIAA Guidance, Navigation, and Control Conference and Exhibit, Keystone, CO, AIAA Paper 2006-6074, 2006.
[44] Prabhakar, A., Fisher, J., and Bhattacharya, R., "Polynomial Chaos Based Analysis of Probabilistic Uncertainty in Hypersonic Flight Dynamics," *Journal of Guidance, Control, and Dynamics*, Vol. 33, No. 1, 2010, pp. 222–234.
doi:10.2514/1.41551
[45] Gill, P. E., Murray, W., and Saunders, M. A., "SNOPT: An SQP Algorithm for Large-Scale Constrained Optimization," *SIAM Journal on Optimization*, Vol. 12, No. 4, 2002, pp. 979–1006.
doi:10.1137/S1052623499350013